





# Analysis of TG-43 dosimetric parameters for an Ir-192 HDR brachytherapy source using with the Geant4 toolkit

Albuquerque<sup>a\*</sup>, A.;  Rosa<sup>a</sup>, L. A. R.;  Souza-Santos<sup>a</sup>, D.

<sup>a,b,c</sup> Instituto de Radioproteção e Dosimetria, Av. Salvador Allende, s/n 22780-160 Rio de Janeiro, RJ, Brasil.

\*Correspondence: alice.asantanna@gmail.com

**Abstract:** This study evaluated the dosimetric parameters of the Buchler G089 <sup>192</sup>Ir high-dose-rate brachytherapy source using the TG-43 formalism and Monte Carlo simulations with the Geant4 toolkit. The radial dose function and the anisotropy function were obtained for this source. For the radial dose function, a small discrepancy could be observed for larger radii. The dose rate constant ( $\Lambda$ ) was also calculated in this study ( $1.114 \text{ cGy}\cdot\text{h}^{-1}\cdot\text{U}^{-1}$ ) showing a maximum relative difference of 0.45% when compared with reference values ( $1.119$  and  $1.115 \text{ cGy}\cdot\text{h}^{-1}\cdot\text{U}^{-1}$ ). The absorbed doses were obtained by positioning the source in the lowest voxel of the ICRP male phantom prostate and benchmarked against previous studies. For comparison criteria, the Amersham 6711-Oncoseed <sup>125</sup>I source was also modeled and inserted in the same position of the prostate. Additionally, the dose enhancement effect due to the presence of gold nanoparticles (GNPs) was analyzed for the <sup>192</sup>Ir source, considering a homogeneous concentration of  $30 \text{ mg}\cdot\text{g}^{-1}$  in a tumor region simulated in the peripheral zone of the prostate. An approximately 18.5% increase in the absorbed dose was observed in this region, in agreement with results from previous studies.

**Keywords:** Geant4, Ir-192, brachytherapy, TG-43 formalism.



# Análise dos parâmetros dosimétricos do TG-43 para uma fonte de braquiterapia HDR Ir-192 usando o kit de ferramentas Geant4

**Resumo:** Este estudo avaliou os parâmetros dosimétricos da fonte de braquiterapia de alta taxa de dose Buchler G089  $^{192}\text{Ir}$  usando o formalismo TG-43 e simulações de Monte Carlo com o kit de ferramentas Geant4. A função de radial de dose e a função de anisotropia foram obtidas para esta fonte. Para a função radial de dose, uma pequena discrepância pôde ser observada para raios maiores. A constante de taxa de dose ( $\Lambda$ ) também foi calculada neste estudo ( $1,114 \text{ cGy}\cdot\text{h}^{-1}\cdot\text{U}^{-1}$ ) mostrando uma diferença relativa máxima de 0,45% quando comparada com valores de referência ( $1,119$  e  $1,115 \text{ cGy}\cdot\text{h}^{-1}\cdot\text{U}^{-1}$ ). As doses absorvidas foram obtidas posicionando a fonte no voxel mais baixo da próstata do simulador masculino da ICRP e comparadas com estudos anteriores. Como critério de comparação a fonte Amersham 6711-Oncoseed de  $^{125}\text{I}$  foi também modelada e inserida na mesma posição da próstata. Adicionalmente, foi analisado o efeito de aumento de dose devido à presença de nanopartículas de ouro (GNPs) para fonte de  $^{192}\text{Ir}$ , considerando uma concentração homogênea de  $30 \text{ mg}\cdot\text{g}^{-1}$  em uma região tumoral simulada na zona periférica da próstata. Observou-se um aumento de aproximadamente 18.5% na dose absorvida nessa região, em concordância com resultados de estudos anteriores.

**Palavras-chave:** Geant4, Ir-192, braquiterapia, formalismo do TG-43.

## 1. INTRODUCTION

According to the World Health Organization (WHO), cancer is among the leading causes of death worldwide before the age of 70 [1]. Current global statistics for 2022 indicate nearly 20 million new cancer cases and approximately 9.7 million cancer-related deaths. Demographic-based projections suggest that the annual number of new cancer cases will rise to 35 million by 2050, representing a 77% increase compared to the estimates for 2022 [2]. Currently, radiotherapy is recommended as part of the treatment for approximately 70% of patients undergoing some form of cancer therapy [3]. The most commonly used radiotherapy modalities are external beam radiotherapy and brachytherapy. Brachytherapy is primarily used for tumors located in easily accessible regions, such as the cervix, oral cavity, and bronchi [4].

Brachytherapy procedures for the treatment of prostate cancer, head and neck cancers, lung cancer, and sarcomas can be either permanent or temporary [5], involving the insertion of catheters to introduce a radioactive source, typically high-dose-rate (HDR)  $^{192}\text{Ir}$  or, less commonly, Co-60, which must be removed after the treatment.

Recently, the incorporation of high-atomic-number ( $Z$ ) metal nanoparticles, such as gold nanoparticles (GNPs), into tumor tissue has been extensively studied through experimental measurements and Monte Carlo (MC) simulations [13][14][15].

The presence of high-atomic-number materials during ionizing radiation therapy generates a considerable increase in the photoelectric absorption cross section in the target tissue, causing a dose-increasing effect and consequently contributing to the potential increase in lethal biological damage.

This technological evolution, however, makes rigorous validation of existing brachytherapy sources even more imperative.

The American Association of Physicists in Medicine (AAPM) Task Group 43 (TG-43) recommends a formalism for calculating dose quantities in water phantoms, defining various dosimetric quantities such as the radial dose function, dose rate constant, and anisotropy function to calculate therapeutic doses for tumors and surrounding tissues with dose constraints to avoid serious damage from the treatment [6].

The different geometries of brachytherapy sources lead to important variations in their dosimetric properties such as anisotropy function ( $F(r,\theta)$ ) and dose rate constant [10]. The Buchler source differs from other  $^{192}\text{Ir}$  sources by having a shorter active core, which results in a significantly lower anisotropy function compared to other sources, such as the microSelectron.

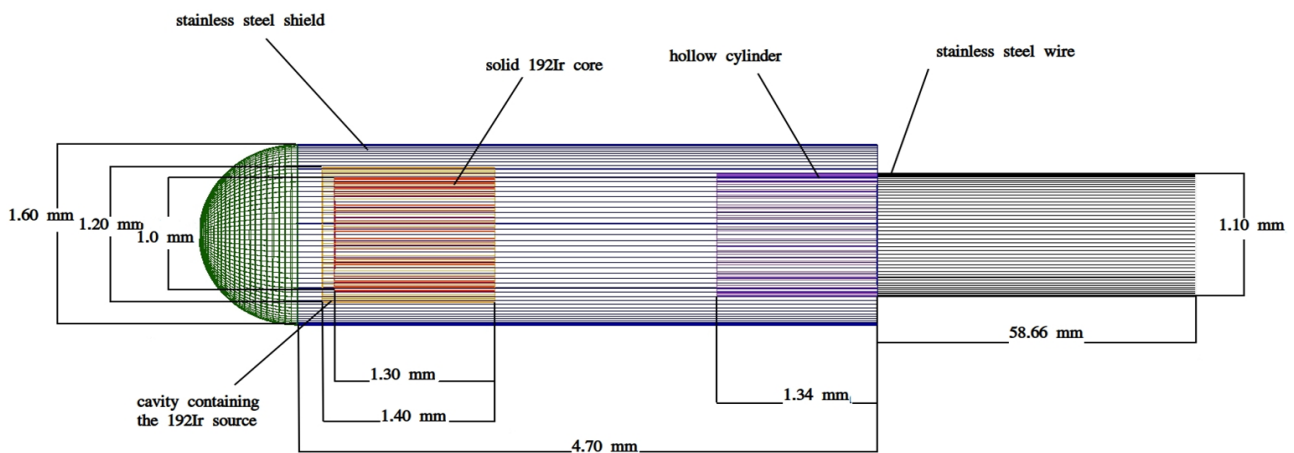
The objective of this work is to characterize Amersham's commercially available  $^{192}\text{Ir}$  source, model Buchler G089, used in brachytherapy treatments. To this end, the dosimetric parameters from the AAPM TG-43 report were calculated using the Geant4 Monte Carlo toolkit. Simultaneously, the study evaluates the performance and accuracy of Geant4 in modeling high-dose-rate brachytherapy sources. Finally, the work explores the absorbed dose distributions of the  $^{192}\text{Ir}$  source and a  $^{125}\text{I}$  reference source in the male ICRP phantom and the influence of GNPs on tumor dose enhancement in a prostate cancer brachytherapy treatment.

## 2. MATERIALS AND METHODS

The brachytherapy source used in this study was the Buchler G089 model developed by Amersham. Its geometry, as seen in Figure 1, consists of a solid  $^{192}\text{Ir}$  core with a diameter of 1 mm and a length of 1.30 mm encapsulated in a stainless steel shield. The end of the shield is a hemisphere with a diameter of 1.60 mm, offset from the center of the source by 0.95 mm. The cavity containing the  $^{192}\text{Ir}$  source is a hollow cylinder with a length of 1.40 mm and inner and outer diameters of 1.20 mm and 1.60 mm, respectively. Adjacent to the

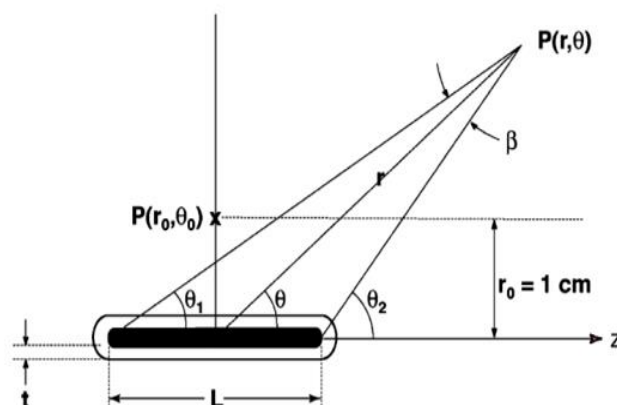
cavity is a solid cylindrical section with a length of 1.76 mm and a diameter of 1.60 mm, followed by a hollow cylinder with a length of 1.34 mm and inner and outer diameters of 1.10 mm and 1.60 mm, respectively. A 6 cm long stainless steel wire is inserted into this hollow section, allowing the source to be inserted into the patient's body. The active length of this source is 1.30 mm.

**Figure 1:** Computational model of the  $^{192}\text{Ir}$  source implemented in Geant4



To assess the source modelling and simulation, we used the mathematical formalism proposed in TG-43, which defines dosimetric quantities in water phantoms such as the radial dose function, dose rate constant, and anisotropy function. Figure 2 in TG-43 is used as a reference for defining the functions outlined by the recommended formalism.

**Figure 2:** Reference for defining functions defined by the formalism recommended by TG 43



Where  $\beta$  is the angle, in radians, between the ends of the linear source and the point of interest  $P(r,\theta)$  relative to the longitudinal axis of the source;  $r$  (cm) is the radial distance from the center of the source to the point of interest  $P(r,\theta)$ ;  $\theta$  (rad) is the angle between the longitudinal axis of the source and the line segment connecting the point of interest to the center of the source and  $L$  (cm) is the active length of the source.

The geometry function has two treatment models: one approximates it as a point source, and the other as an extended linear source. In our case, we use the geometry function for linear sources, according to equation (1).

$$G_L(r, \theta) = \left\{ \frac{\beta}{Lr \sin \theta} \text{ if } \theta \neq 0^\circ \right\}; G_L(r, \theta) = \left\{ \left( r^2 - \frac{L^2}{4} \right)^{-1} \text{ if } \theta = 0^\circ \right\} \quad (1)$$

The radial dose function,  $g(r,\theta)$ , accounts for dose falloff in the transverse plane, considering scattered and attenuated photons in the medium while excluding the geometric function component. This function is defined by equation (2), where  $r_0 = 1$  cm and  $\theta_0 = \pi/2$ :

$$g_x(r) = \frac{\dot{D}(r,\theta) G_x(r_0,\theta_0)}{\dot{D}(r_0,\theta_0) G_x(r,\theta_0)} \quad (2)$$

The anisotropy function characterizes the anisotropic distribution of the dose in a medium surrounding the radiation source. Physically, this function incorporates the effects of scattering and attenuation, representing the variation of the dose as a function of the angles relative to the transverse plane. Mathematically, the anisotropy function can be determined by equation (3):

$$F(r, \theta) = \frac{\dot{D}(r,\theta) G_L(r,\theta_0)}{\dot{D}(r,\theta_0) G_L(r,\theta)} \quad (3)$$

To evaluate the Buchler source, its modeling was implemented in Geant4, as shown in Figure 1. The dose was then simulated for 36 different radii ranging from 0.2 cm to 20 cm using a  $10^8$  Monte Carlo histories. The radial dose function and anisotropy function parameters were then obtained from the dose and compared with those obtained by Taylor et al. [7].

The air kerma strength,  $S_k$ , is the air-kerma rate at distance  $d$ , used here as 1 m for the Monte Carlo calculations, in vacuo and due to photons of energy greater than  $d$  multiplied by the square of the distance  $d$ , as in equation (4):

$$S_k = \dot{K}_\delta(d) \cdot d^2 \quad (4)$$

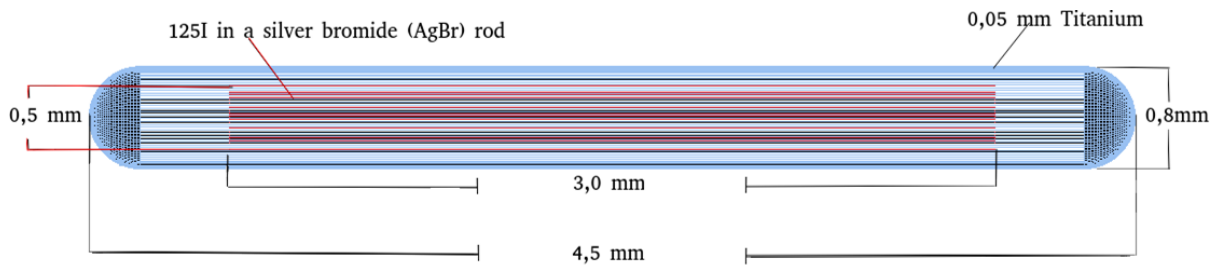
The dose rate constant represents the dose rate in water at the reference point one centimeter from the transverse axis per unit air kerma force. In this study, the dose rate constant evaluated with Geant4 was benchmarked against previously published results by Ballester [8] and Rogers [7]. This quantity can be obtained from the air kerma strength,  $S_k$ , as in equation (5):

$$\Lambda = \frac{\dot{D}(r_0, \theta_0)}{S_k} \quad (5)$$

After evaluation using the TG-43 formalism, the source was positioned in the prostate region of the ICRP male anthropomorphic voxel phantom [9]. The doses delivered to the prostate and neighboring organs were obtained using Monte Carlo simulation with Geant4 and the results were then compared with those of Martins *et al.* [12], who used a different phantom developed by Zubal *et al.* [11]. While the ICRP phantom is composed of voxels measuring  $2.137 \times 2.137 \times 8 \text{ mm}^3$ , the Zubal phantom uses voxels measuring  $3.6 \times 3.6 \times 3.6 \text{ mm}^3$ . Furthermore, the Zubal model includes only the head and torso, unlike the ICRP phantom, which represents a complete adult male with legs and arms. Additional differences are observed in organ volumes, as shown in Table 2.

For comparison purposes, the  $^{125}\text{I}$  Amersham 6711 - Oncoseed source was also modeled and inserted in the same prostate position as the ICRP phantom. Absorbed doses were obtained using the Geant4 toolkit and compared with doses obtained in previous studies [12] and with the doses obtained for the  $^{192}\text{Ir}$  source in this study.

**Figure 3:** Computational model of the  $^{125}\text{I}$  source implemented in Geant4



The Oncoseed source is made by absorbing  $^{125}\text{I}$  in a silver bromide (AgBr) rod with a 2.5:1 AgBr:AgI ratio and a density of  $6.2 \text{ g/cm}^3$ . The core is encapsulated in titanium and laser-sealed. This seed is 4.5 mm long and 0.8 mm in diameter.

To complement the analysis of the  $^{192}\text{Ir}$  source and in line with advances in studies on dose escalation in brachytherapy treatments in the presence of GNPs, a tumor-simulating region was included in the Peripheral Zone (PZ) of the prostate of the ICRP phantom. This region was selected due to the high incidence of prostate cancer (70-80% of cases) in this location [16]. The tumor volume was filled with a homogeneous concentration of 30 mg of gold per gram of tissue, a ratio adopted in previous studies of dose enhancement due to the presence of GNPs in water phantoms [13][14][15].

In this study, the absorbed doses in this volume were obtained and compared with the absorbed dose without the presence of GNPs. For this purpose, the  $^{192}\text{Ir}$  source was positioned 1 cm from the tumor region.

The effect of GNPs was evaluated using the dose enhancement factor (DEF), defined as the ratio of the total dose administered in the volume in the presence of GNPs to the total dose in the same volume without the presence of GNPs. As in equation (6):

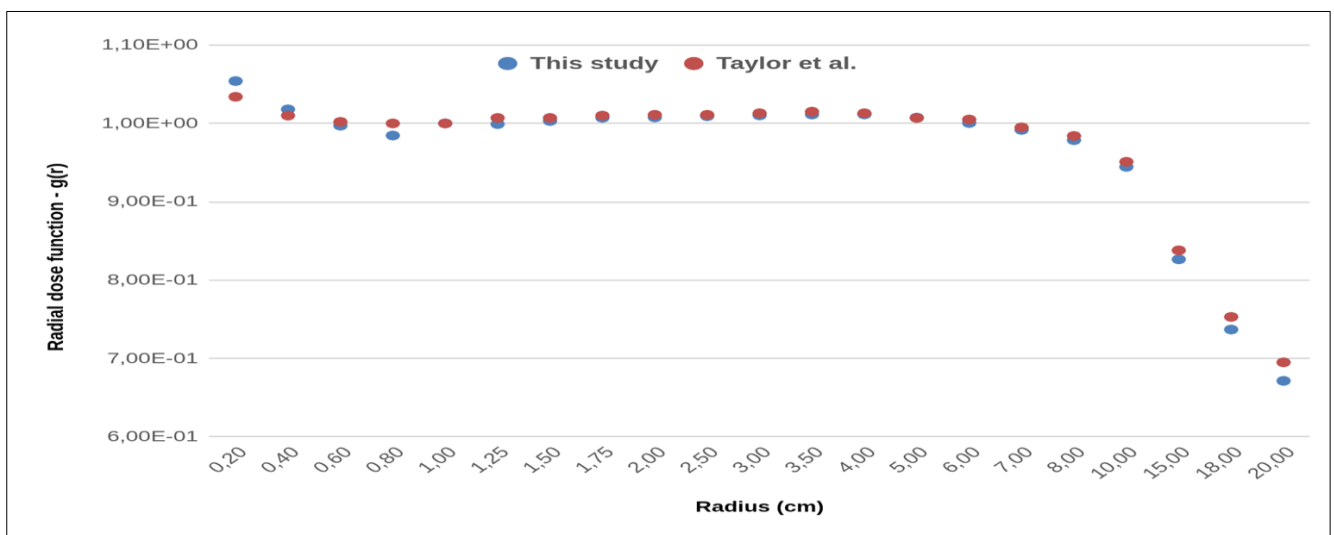
$$DEF = \frac{D_{withGNPs}}{D_{withoutGNPs}} \quad (6)$$



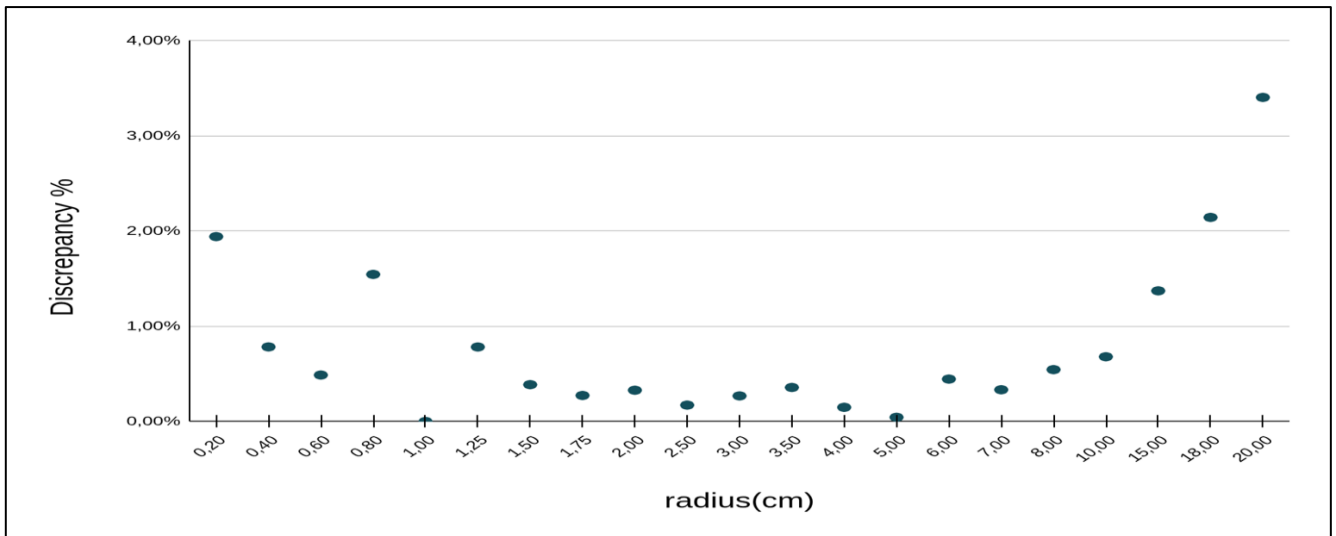
### 3. RESULTS AND DISCUSSIONS

Figure 4 illustrates the radial dose function (RDF) of the Buchler  $^{192}\text{Ir}$  source, comparing results from Geant4 Monte Carlo simulations with data obtained by Taylor et al. [7]. The simulation was conducted in a cylindrical water phantom for 36 radial distances, ranging from 0.2 cm to 20 cm, using a reference radius of 1 cm and an angle of  $\theta = \pi/2$ . The simulated results demonstrated good agreement with Taylor et al. [7], particularly at distances close to the source. A slight divergence was observed at larger radial distances as shown in Figure 5, which depicts the percentage discrepancies.

**Figure 4:** Comparison of the Radial Dose Function obtained through simulation with Geant4 and reference results.



**Figure 5:** Relative percentage discrepancy for values obtained for radial dose function



Figures 6 to 13 present the anisotropy function for the Buchler <sup>192</sup>Ir source at radii of 0.25 cm, 0.50 cm, 3.00 cm, 5.00 cm, 7.50 cm, 10.00 cm, 12.50 cm, and 20.00 cm, respectively. The anisotropy function results obtained through Geant4 simulations were compared with the reference data provided by Taylor et al. [7]. The analysis shows good agreement between the simulated and reference values across all radii. At smaller radii (Figure 6 and 7), minor deviations are observed near the longitudinal axis of the source. For larger radii (Figures 11 to 13), the anisotropy function stabilizes, with discrepancies decreasing as the distance increases.

Table 1 shows dose rate constant values ( $\Lambda$ ) obtained in this study (1.114 cGy·h<sup>-1</sup>·U<sup>-1</sup>) showed consistency with those reported by Taylor et al. [7] (1.119 cGy·h<sup>-1</sup>·U<sup>-1</sup>) and Ballester et al. [8] (1.115 cGy·h<sup>-1</sup>·U<sup>-1</sup>), with a maximum relative difference of 0.45%.

**Table 1:** Comparison of the dose rate constant ( $\Lambda$ ) values for the Buchler <sup>192</sup>Ir brachytherapy source obtained in this study with reference results.

	Taylor et al. [7]	Ballester et al. [8]	This study
$\Lambda$ (cGy h <sup>-1</sup> U <sup>-1</sup> )	1.119	1.115	1.114

Table 2 compares the absorbed doses calculated using Geant4 for the prostate, testes, urinary bladder wall, and rectum with the reference values reported by Martins et al. [12]. It is

important to note here that the reference results are obtained for the Zubal phantom, while the ICRP male phantom was used in the present study. Nevertheless, the doses calculated for the  $^{192}\text{Ir}$  source have the same order of magnitude as the reference values, even though the Zubal phantom does not contain the lower legs and has significantly different voxel dimensions and organ volumes when compared to the dimensions and volumes of the ICRP phantom.

**Figure 6 to 13:** Comparison of the Anisotropy Function obtained through simulation with Geant4 and reference results for radii of 0.25cm, 0.50cm, 3.00cm, 5.00cm, 7.50cm, 10.00cm, 12.50cm and 20.00cm respectively.

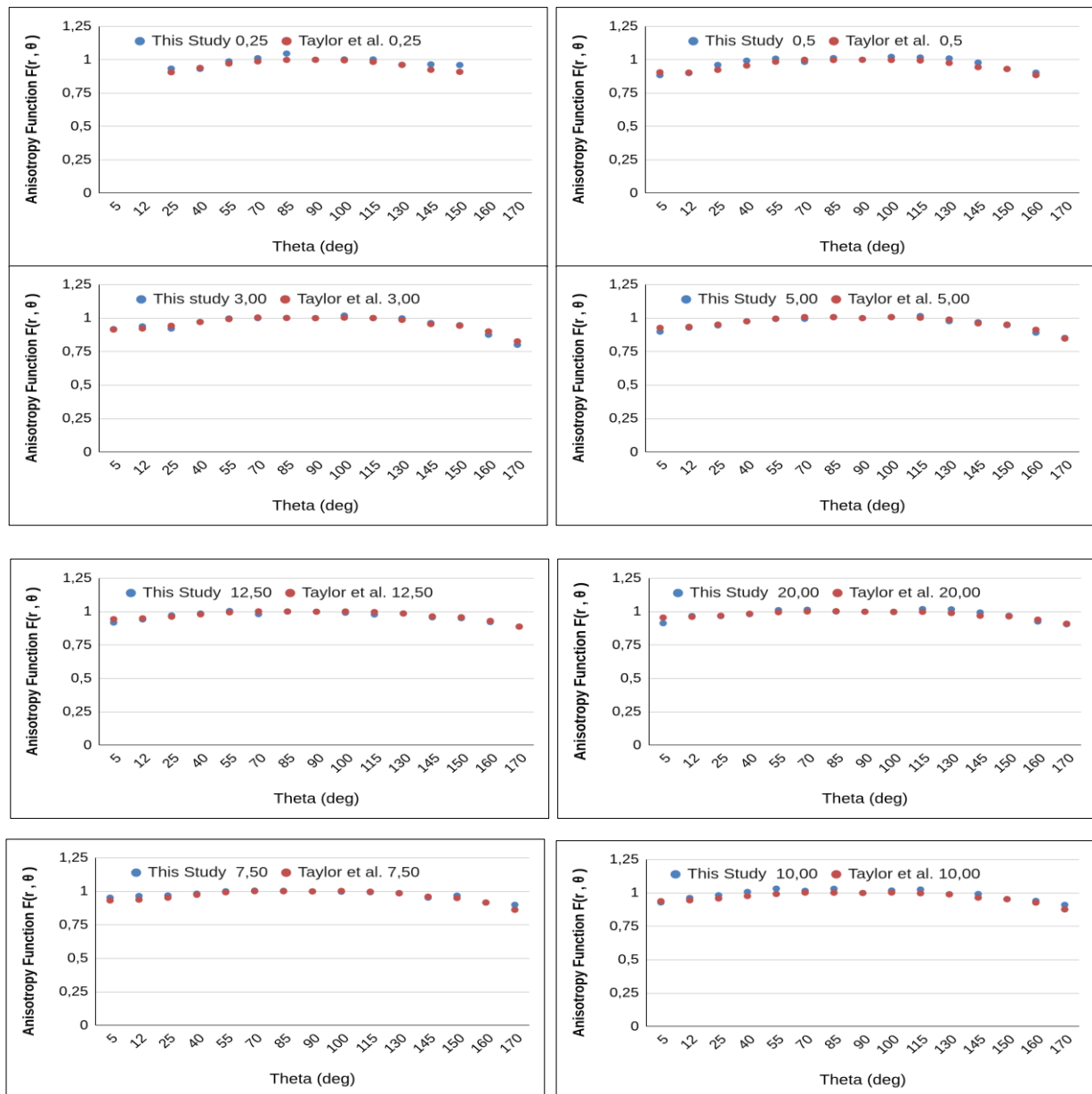


**Table 2:** Absorbed dose per photon (Gy/photon) and phantom organ volumes using Geant4 for the  $^{192}\text{Ir}$  Buchler source, compared with reference values.

Organ	Geant4 – Dose/Photon(Gy)	Martins et. al. Dose/Photon(Gy)	Volume ICRP (cm <sup>3</sup> )	Volume Zubal (cm <sup>3</sup> )
Prostate	6,49E-14	4,49E-14	16,51	20,44
Urinary Bladder wall	2,58E-15	1,43E-15	48,08	146,83
Testes	1,48E-15	1,56E-15	33,65	69,00
Rectum	3,04E-15	5,24E-15	28,83	68,44

The absorbed doses were also obtained for the  $^{125}\text{I}$  Oncoseed source used in LDR treatments. This source was modeled and positioned in the same prostate voxel as the  $^{192}\text{Ir}$  source. The results obtained for the prostate and organs at risk can be seen in Table 3, which compares the absorbed doses calculated using Geant4 with the results reported by Martins et al. for the same source.

**Table 3:** Absorbed dose per photon (Gy/photon) from this study using Geant4 toolkit for the  $^{125}\text{I}$  source, compared with Martins et al. [12] values.

Organ	Geant4 - Dose/Photon(Gy)	Martins et. al. Dose/Photon(Gy)
Prostate	1,66E-14	1,62E-14
Urinary Bladder wall	4,72E-16	8,57E-17
Testes	1,67E-16	1,37E-16
Rectum	0,69E-15	1,22E-15

The large difference observed between the results by Martins et al. and this work for the Urinary bladder wall, showing a factor of almost 5 between both values is hard to explain just by geometrical reasoning. A possible explanation is if the authors included the urine mass in the dose calculation. If we do the same, our result for the urinary bladder becomes  $8,48 \times 10^{-17}$  Gy, presenting a difference of less than 1% to their value.

Table 4 shows the comparison between the absorbed doses per photon (Gy/photon) for the  $^{192}\text{Ir}$  (HDR) and  $^{125}\text{I}$  (LDR) sources simulated in the ICRP phantom for prostate, testicles and urinary bladder wall. In both cases, the prostate presents the highest relative

dose, demonstrating adequate concentration of the dose distribution in the target volume. However, significant differences can be observed in the surrounding organs.

For the  $^{192}\text{Ir}$  source, the relative doses to the bladder, rectum, and testicles are higher, which is explained by the higher average photon energy ( $\sim 380$  keV). In contrast, the  $^{125}\text{I}$  source ( $\sim 28$  keV), presents a more localized distribution and marked attenuation in the tissues, reducing the relative dose to the organs at risk.

**Table 4 :** Absorbed dose per photon (Gy/photon) from this study using Geant4 toolkit for the  $^{192}\text{Ir}$  source, compared with the  $^{125}\text{I}$  source values.

Organ	Dose/photon (Gy) ICRP $^{192}\text{Ir}$	Dose/photon (Gy) ICRP $^{125}\text{I}$	Organ to prostate dose ratios with $^{192}\text{Ir}$	Organ to prostate dose ratios with $^{125}\text{I}$
Prostate	6,49E-14	1,66E-14	1,00E+00	1,00E+00
Urinary Bladder wall	2,58E-15	4,72E-16	3,98E-02	2,84E-02
Testes	1,48E-15	1,67E-16	2,28E-02	1,01E-02
Rectum	3,04E-15	6,19E-16	4,68E-02	3,73E-02

Table 5 shows the dose increase (DEF) due to the presence of GNPs at a homogeneous concentration of 30 mg/g in the healthy region of the prostate and in the tumor for the  $^{192}\text{Ir}$  source. It can be observed that for this concentration, there was a 18% dose increase in the tumor region containing the GNP concentration. In the prostate tissue surrounding the tumor, the dose is preserved.

**Table 5 :** Absorbed dose per photon (Gy/photon) with and without the presence of GNPs and DEF obtained using the Geant4 toolkit for the  $^{192}\text{Ir}$  source.

Organ	Dose (Gy) with 30mg/g	Dose (Gy) without GNPs	DEF(30mg/g)
Prostate	4,14E-14	4,16E-14	0,995
Tumor	2,49E-13	2,11E-13	1,185

In a previous study [13], the dose enhancement (DEF) due to the presence of GNPs was analyzed for a cubic phantom ( $30\text{ cm}^3$ ) of water in voxels containing the modeling of an  $^{192}\text{Ir}$  source and a  $1\text{ cm}^3$  tumor region. The DEF for a concentration of 30 mg/g obtained by Zabihzadeh et.al was 1.194, which represents a relative discrepancy of 0.838% in relation to the present study (1.184).

## 4. CONCLUSIONS

The results obtained with the Geant4 Monte Carlo simulation demonstrate consistency with the reference values for the radial dose function and anisotropy function of the Buchler  $^{192}\text{Ir}$  brachytherapy source. The absorbed doses calculated for the prostate, testes, urinary bladder wall, and rectum, compared to the reference values reported by Martins *et al.* [12], confirming the reliability of the simulation in accurately evaluating dose distributions.

Additionally, the dose rate constant ( $\Lambda$ ) obtained in this study ( $1.114 \text{ cGy}\cdot\text{h}^{-1}\cdot\text{U}^{-1}$ ) exhibited a maximum relative difference of 0.45% with previously reported values by Taylor *et al.* [7] ( $1.119 \text{ cGy}\cdot\text{h}^{-1}\cdot\text{U}^{-1}$ ) and Ballester *et al.* [8] ( $1.115 \text{ cGy}\cdot\text{h}^{-1}\cdot\text{U}^{-1}$ ).

The results obtained comparing the  $^{192}\text{Ir}$  source with the  $^{125}\text{I}$  source demonstrate consistency with what is expected from the literature regarding differences between treatment types. Although the prostate receives the highest relative dose in both scenarios, the energy differences between the sources result in distinct dosimetric profiles. Due to its higher average energy,  $^{192}\text{Ir}$  presents greater penetration, resulting in higher doses in adjacent organs, while  $^{125}\text{I}$  promotes more localized distribution, with relatively lower doses in organs at risk.

Considering the prostate as the planning target volume (PTV) and its affected region as the gross tumor volume (GTV), a procedure commonly adopted in prostate brachytherapy, the results indicate an 18.5% dose increase in the latter region when GNPs are used in the affected region with the  $^{192}\text{Ir}$  source. These results are consistent with the results of previous studies [13]. At the same time, the dose in the PTV region beyond the GTV presents a very small variation when compared to the dose in the same region without the use of GNPs; in fact, there is a dose reduction in this region of 0.5%. This indicates the possibility of reducing the treatment dose, since GNPs will increase the dose in the GTV to values adequate for tumor control, and the dose in the prostate region beyond the GTV would be lower. Furthermore, a reduction in the treatment dose would contribute to a reduction in the dose to healthy organs, such as the bladder and rectum.

It is important to emphasize that previous studies have not analyzed dose enhancement in the presence of GNPs in complex anthropomorphic phantoms in voxel like the ICRP phantom used in this study. However, further studies using other concentrations and other organs are needed for a more precise analysis of the effect of dose enhancement.

Although this study does not intend to delve deeper into the analysis of the influence of GNPs on brachytherapy treatments, source validation using TG-43 is extremely important so that more in-depth studies using the same modeling can further investigate these findings.

These findings emphasize the robustness of the Geant4 simulation toolkit for the purpose of brachytherapy treatment planning. Nevertheless, further studies are necessary to refine dose calculations, particularly by exploring the impact of electron production cuts at larger radii and in organ dose assessments in different anthropomorphic phantoms, such as mesh phantoms.

## ACKNOWLEDGMENT

The authors thank Mr. Delano Valdivino Santos Batista, Medical Physicist, M.Sc., for the fruitful discussions.

## FUNDING

The Authors reports financial support was provided by the Coordenação de Aperfeiçoamento de Pessoal de Nível Superior– Brasil (CAPES) – Finance Code 001. Process number: 88887.605030/2021-00.

## CONFLICT OF INTEREST

All authors declare that they have no conflicts of interest

## REFERENCES

- [1] FERLAY, J. et al. Cancer statistics for the year 2020: An overview. *International Journal of Cancer*, v. 149, n. 4, p. 778-789, 2021.
- [2] BRAY, Freddie et al. Global cancer statistics 2022: GLOBOCAN estimates of incidence and mortality worldwide for 36 cancers in 185 countries. *CA: A Cancer Journal for Clinicians*, v. 74, n. 3, p. 229-263, 2024.
- [3] SCOTT, Jacob G. et al. Personalizing radiotherapy prescription dose using genomic markers of radiosensitivity and normal tissue toxicity in NSCLC. *Journal of Thoracic Oncology*, v. 16, n. 3, p. 428-438, 2021.
- [4] MARTAI, Gustavo Nader et al. Câncer de próstata localizado: teleterapia, braquiterapia ou prostatectomia radical?. *Diagn Tratamento*, v. 17, n. 2, 2012.
- [5] LEVITTI, Seymour H. et al. *Technical basis of radiation therapy*. Berlin Heidelberg: Springer, 2012.
- [6] RIVARD, Mark J. et al. Update of AAPM Task Group No. 43 Report: A revised AAPM protocol for brachytherapy dose calculations. *Medical Physics*, v. 31, n. 3, p. 633-674, 2004.
- [7] TAYLOR, R. E. P.; ROGERS, D. W. O. An EGSnrc Monte Carlo-calculated database of TG-43 parameters. *Medical Physics*, v. 35, p. 4228-4241, 2008.
- [8] BALLESTER, F. et al. Monte Carlo dosimetry of the Buchler high dose rate <sup>192</sup>Ir source. *Physics in Medicine & Biology*, v. 46, n. 3, p. N79, 2001.7
- [9] ICRP. Adult reference computational phantoms. ICRP Publication 110. *Ann. ICRP*, v. 39, n. 2, p. 1, 2009.
- [10] PAPAGIANNIS, P. et al. Dosimetry comparison of sources. *Medical Physics*, v. 29, n. 10, p. 2239-2246, 2002.
- [11] I.G.. Zubal, C.R Harrell, E.O Smith,, Rattner, Z., Gindi, G. and Hoffer, P.B., “Computerized three-dimensional segmented human anatomy”, *Medical Physics*, Vol 21(2):299-302, 1994;
- [12] MARTINS, Maximiano C. et al. Study of dose distributions in voxel phantoms for brachytherapy sources using the GEANT4 Monte Carlo toolkit. 2009.



- [13] ZABIHZADEH, Mansour; AREFIAN, Sahar. Tumor dose enhancement by nanoparticles during high dose rate  $^{192}\text{Ir}$  brachytherapy. *Journal of cancer research and therapeutics*, v. 11, n. 4, p. 752-759, 2015.
- [14] CHO, Sungkoo et al. Monte Carlo simulation study on dose enhancement by gold nanoparticles in brachytherapy. *J Korean Phys Soc*, v. 56, n. 6, p. 1754-1758, 2010.
- [15] AL-MUSYWEL, H. A.; LAREF, A. Effect of gold nanoparticles on radiation doses in tumor treatment: a Monte Carlo study. *Lasers in Medical Science*, v. 32, n. 9, p. 2073-2080, 2017.
- [16] JAFARI-SALES, Abolfazl et al. A Comprehensive Study of Prostate Cancer and Epstein-Barr Virus Infection: A Systematic Review and Meta-analysis. *Iranian Journal of Blood and Cancer*, v. 17, n. 2, p. 58-69, 2025.

---

## LICENSE

This article is licensed under a Creative Commons Attribution 4.0 International License, which permits use, sharing, adaptation, distribution and reproduction in any medium or format, as long as you give appropriate credit to the original author(s) and the source, provide a link to the Creative Commons license, and indicate if changes were made. The images or other third-party material in this article are included in the article's Creative Commons license, unless indicated otherwise in a credit line to the material.

To view a copy of this license, visit <http://creativecommons.org/licenses/by/4.0/>.